

Modern Physics Letters B  
© World Scientific Publishing Company

## Understanding all-optical spin switching: Comparison between experiment and theory

G. P. Zhang\* and M. Murakami

*Department of Physics, Indiana State University, Terre Haute, IN 47809, USA*

*\*gpzhang.physics@gmail.com*

M. S. Si

*Key Lab for Magnetism and Magnetic Materials of the Ministry of Education, Lanzhou University, Lanzhou 730000, China*

Y. H. Bai

*Office of Information Technology, Indiana State University, Terre Haute, IN 47809, USA*

Thomas F. George

*Office of the Chancellor, Departments of Chemistry & Biochemistry and Physics & Astronomy University of Missouri-St. Louis, St. Louis, MO 63121, USA*

Received (March 24, 2022)

Revised (Day Month Year)

Information technology depends on how one can control and manipulate signals accurately and quickly. Transistors are at the core of modern technology and are based on electron charges. But as the device dimension shrinks, heating becomes a major problem. The spintronics explores the spin degree of electrons and thus bypasses the heat, at least in principle. For this reason, spin-based technology offers a possible solution. In this review, we survey some of latest developments in all-optical switching (AOS), where ultrafast laser pulses are able to reverse spins from one direction to the other deterministically. But AOS only occurs in a special group of magnetic samples and within a narrow window of laser parameters. Some samples need multiple pulses to switch spins, while others need a single-shot pulse. To this end, there are several models available, but the underlying mechanism is still under debate. This review is different from other prior reviews in two aspects. First, we sacrifice the completeness of reviewing existing studies, while focusing on a limited set of experimental results that are highly reproducible in different labs and provide actual switched magnetic domain images. Second, we extract the common features from existing experiments that are critical to AOS, without favoring a particular switching mechanism. We emphasize that given the limited experimental data, it is really premature to identify a unified mechanism. We compare these features with our own model prediction, without resorting to a phenomenological scheme. We hope that this review serves the broad readership well.

*Keywords:* All-optical switching, spin dynamics, dynamic simulation

2 *Zhang, Murakami, Si, Bai, and George*

## 1. Introduction

Computing technology demands high-speed operation and miniaturization of computing bits.<sup>1</sup> It is remarkable that the computer clock frequency has improved steadily for the last decade, but then has plateaued around 2005, because the simple constant-electric field scaling rules break down.<sup>2</sup> Both technical constraints (physics) and cost constraints (economics) are responsible for the clock frequency plateau.<sup>2</sup> In the constant-field scaling, the threshold voltage must be reduced as the clock frequency increases, but this very reduction results in increase in OFF current, which is unacceptable to maintain a high ON/OFF current ratio. The second problem is associated with the gate insulator thickness reduction, which increases gate current leakage. A way out of this is to use the constant voltage scaling. But it comes with an huge increase in areal power density. So this is unsustainable.<sup>2</sup> To meet the insatiable demand on computing technology, one must pursue other means.

All-optical spin switching (AOS)<sup>3</sup> combines the speed<sup>4</sup> that an ultrafast laser pulse delivers and the powerful storage capability that existing magnetic media offer, yet free of a magnetic field. It is still at the early stage of development, but results are promising. Figure 1 schematically shows several possible switching channels. In general, AOS can be classified into two broad categories, depending on how the helicity affects AOS and how many laser pulses are needed to switch spins, respectively. The first category refers to the helicity-dependent all-optical switching, HD-AOS, where the right-circularly polarized light ( $\sigma^+$ ) switches a spin from up to down, while the left-circularly polarized light ( $\sigma^-$ ) from down to up. The linearly polarized light ( $\pi$ ) only creates multidomains, with mixed up and down spins. By contrast, in the helicity-independent all-optical switching, HID-AOS,  $\sigma^+$ ,  $\sigma^-$  and  $\pi$  all switch spins. This is in contrast to ordinary thermomagnetic switching due to local laser heating and dipolar interactions, where it only leads to a one-time reversal without switching back the spins.<sup>5</sup>

Besides the above elementary operations, AOS is found highly laser- and material-specific, where often one finds that spins in the same type of materials are both switched optically and electrically. A large fraction of AOS materials require multiple pulses to switch spins. So far, only four types of materials – GdFeCo,<sup>6</sup> Pt/Co/Gd,<sup>7</sup> Co/Pt/Co/GdFeCo,<sup>8</sup> and Pt/Co/Pt<sup>9</sup> – allow a single shot switching (see Fig. 1). They are among the most promising materials to be used in the future, and they can create tunable topological magnetic structures such as Skyrmions.<sup>10</sup>

There are several excellent review articles available. Kirilyuk and coworkers<sup>11</sup> reviewed the status of the field before 2010, which is quite comprehensive and includes other branches of femtomagnetism.<sup>12</sup> Two newer reviews<sup>13,14</sup> cover major parts of prior research in this field. Our current review does not aim to be comprehensive, so we regret that many excellent references can not be cited. The review instead complements the prior reviews by focusing on highly reproducible experiments where magnetic domain images are taken. As research is ongoing,<sup>15</sup> we

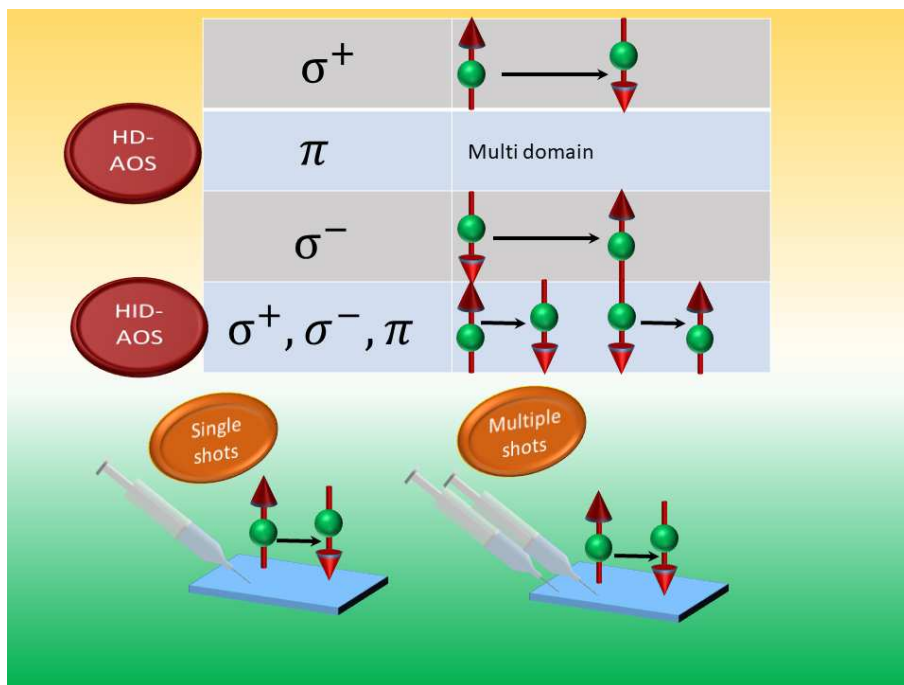


Fig. 1. Overview of all-optical spin switching. Based on the laser helicity, one can distinguish two major kinds of AOS: One is helicity-dependent and the other is helicity-independent. Based on the number of pulses used in switching, there are single-shot and multiple-shot switchings.

consider our review as an alternative to the existing understanding of AOS.

The rest of the paper is arranged as follows. In Sec. II, we briefly review the history of AOS<sup>3</sup> but focus on those specific materials that allow AOS. These materials are provided in a table for the reader, with hope to find a common feature among all AOS materials. Section III is devoted to the role of the spin moment and spin configuration in AOS, where we discuss how materials do not switch, impact of reduced dimensionality, a practical method of extraction of spin angular momentum from experimental data, and dynamical simulation. In Sec. IV, we present a simple theory for all-optical switching, where we connect the inverse Faraday theory with our model and first-principles results. Section V highlights the significance of orbital angular momentum on perpendicular magnetic anisotropy and AOS. Section VI is based on the latest experimental results in single-shot AOS ferromagnets. Finally, we conclude this paper in Sec. VII.

## 2. Discovery of AOS

In 2007, Stanciu and coworkers<sup>3</sup> discovered that exposing a ferrimagnet  $\text{Gd}_{22}\text{Fe}_{74.6}\text{Co}_{3.4}$  to a 40-fs 800-nm laser pulse creates a permanent spin reversal. The images of magnetic domains, before and after laser excitation, record the re-

markable switching. The right-circularly polarized light ( $\sigma^+$ ) switches the down domain to the up domain. If the magnetic domain is already up, then there is no effect on the domain. The left-circularly polarized light ( $\sigma^-$ ) switches the up domain to down domain and has no effect on the down domain. If a domain is exposed to linearly polarized light ( $\pi$ ), it does not switch, but instead breaks the original domain into smaller domains randomly oriented up or down. Its broad appeal to both materials scientists, and optical and electric engineers is almost immediate and results in plenty of experimental investigations.

For a long time, ferrimagnetic rare-earth transition metal alloys<sup>3,16</sup> have remained the only material showing AOS. This led some researchers to speculate the crucial role of antiferromagnetic orders between the rare-earth and transition-metal sublattices. By contrast, many antiferromagnetic materials, such as  $\text{TmFeO}_3$ <sup>17</sup> and  $\text{DyFeO}_3$ ,<sup>18</sup> which have a “correct” coupling, do not switch their spins permanently; instead, they only reorient their spins. To get a glimpse of the hot debates among different research groups, in Table 1 we list 31 most intensively investigated AOS compounds, together with 4 non-AOS compounds (first four entries). We also list magnetic orderings, underlying mechanisms proposed or disproved (the entries with slanted lines), and whether the switching is HD-AOS or HID-AOS. Unfortunately, not all the studies have discussed the underlying mechanism, so we leave them blank. In some cases, several mechanisms are proposed, but we only choose one or two. The acronyms are explained in the caption of the table. These 4 non-AOS compounds are used as a counter-example that antiferromagnetic ordering and the inverse-Faraday effect may not be enough for AOS. All 31 AOS compounds have actual magnetic domain images taken before and after laser exposure. We specifically avoid materials that only one or two groups are familiar with.

This table is particularly important. Several common themes appear and can be summarized as follows:

Table 1. Chronicle of AOS materials whose magnetic domain images are taken. Ordering refers to magnetic ordering. IFE: inverse Faraday effect. SF-SRS: spin-flip stimulated Raman scattering. FIM: ferrimagnetic. AFM: antiferromagnetic. PM: paramagnetic. Under Mechanism, only a selected few are listed. Linear: linear reversal; HD-AOS: helicity-dependent all-optical switching; HID-AOS: helicity-independent all-optical switching;  $T_{\text{comp}}$ : compensation temperature dependent; MCD: magnetic circular dichroism; SDC: superdiffusive current; LR: low remanence; DM: magnetic domain size; ST: stochastic. These underlined compounds are the only ferromagnets that show a single-shot switching. The slanted lines denote those that are disapproved by a referenced paper.

Compound	Ordering	Mechanism	AOS/Non-AOS	Ref.
TmFeO <sub>3</sub>	AFM		Non-AOS	17
DyFeO <sub>3</sub>	AFM	IFE	Non-AOS	18
HoFeO <sub>3</sub>	AFM	IFE	Non-AOS	19
NaTb(WO <sub>4</sub> ) <sub>2</sub>	PM	IFE	Non-AOS	20
Gd <sub>22</sub> Fe <sub>74.6</sub> Co <sub>3.4</sub>	FIM	IFE	HD-AOS	3
Gd <sub>22</sub> Fe <sub>74.6</sub> Co <sub>3.4</sub>	FIM	<del>Thermal</del>	AOS	21
Gd <sub>24</sub> Fe <sub>66.5</sub> Co <sub>9.5</sub>	FIM	Linear	HD-AOS	22
Gd <sub>26</sub> Fe <sub>64.7</sub> Co <sub>9.3</sub>	FIM	<u>IFE/SF-SRS</u>	HD-AOS	23
Gd <sub>23</sub> Fe <sub>68</sub> Co <sub>9</sub>	FIM	IFE	HD-AOS	24
Gd <sub><math>x=20 \leftrightarrow 28</math></sub> Fe <sub>90-x</sub> Co <sub>10</sub>	FIM	IFE/Linear	H(I)D-AOS	25
Gd <sub>26</sub> Fe <sub>65</sub> Co <sub>9</sub>	FIM	MCD	HD-AOS	26
Gd <sub>24,25</sub> Fe <sub>66.5</sub> Co <sub>9.5</sub>	FIM	Thermal	HID-AOS	6
Gd <sub>24,25</sub> Fe <sub>65.6</sub> Co <sub>9.4</sub>	FIM	Thermal	HID-AOS	6
Gd <sub>24</sub> Fe <sub>66.5</sub> Co <sub>9.5</sub>	FIM		H(I)D-AOS	27
Tb <sub><math>x=0.12 \leftrightarrow 0.34</math></sub> Co <sub>1-x</sub>	FIM	$T_{\text{comp}}$	H(I)D-AOS	28
Tb <sub><math>x=19 \leftrightarrow 38.5</math></sub> Fe <sub>100-x</sub>	FIM	<del><math>T_{\text{comp}}</math></del>	HD-AOS	29
Co/Ir/CoNiPtCo/Ir,Tb <sub>26</sub> Co <sub>74</sub>	FIM	$T_{\text{comp}}$	HD-AOS	30
Tb/Co multilayer	FIM	$T_{\text{comp}}$	HD-AOS	30
Tb <sub>36</sub> Fe <sub>64</sub> /Tb <sub>19</sub> Fe <sub>81</sub>	FIM	LR	HD-AOS	31
Tb <sub>29</sub> Fe <sub>71</sub> ,Tb <sub>34</sub> Fe <sub>66</sub>	FIM	LR	HD-AOS	32
Tb <sub>30</sub> Fe <sub>70</sub>	FIM	conductivity	HD-AOS	33
Tb <sub>22</sub> Fe <sub>69</sub> Co <sub>9</sub>	FIM	<del>IFE,MCD</del>	HD-AOS	34
Tb <sub><math>x=8 \rightarrow 14.5</math></sub> Co <sub>100-x</sub> (< 6.5nm)	FIM	DM, <del>LR</del>	HD-AOS	35
Tb <sub><math>x=16.5 \rightarrow 30.5</math></sub> Co <sub>100-x</sub> (< 15nm)	FIM	DM, <del>LR</del>	HD-AOS	35
Tb <sub><math>x=22 \rightarrow 34</math></sub> Fe <sub>100-x</sub> (5-85nm)	FIM	LR	HD-AOS	36
Pt/Co/Gd	FIM	Thermal	HID-AOS	7
[Co(4Å)/Pt(7Å)] <sub>2→3</sub>	FM		HD-AOS	37
Pt/Co(6Å ↔ 15Å)/Pt	FM		HD-AOS	37
[Pt/Co <sub>1-x</sub> Ni <sub>x</sub> (6Å)] <sub>2→4</sub>	FM		HD-AOS	37
Cu/[Ni(5Å)/Co(1Å)] <sub>2</sub> /Ni/Cu	FM	<del>SDC</del>	HD-AOS	37
[Co(2Å)/Ni(6Å)] <sub>2</sub>	FM	DM	HD-AOS	35
[Pt(7Å)/Co(6Å)] <sub>1-2</sub>	FM	DM	HD-AOS	35
FePt	FM	ST	HD-AOS	38
Co/Pt/Co/GdFeCo	FIM/FM	<del>transport</del>	HID-AOS	8
[Co/Pt]/Cu/GdFeCo	FIM/FM	transport	HID-AOS	39
Pt/Co/Pt	FM	<del>IFE</del>	HID-AOS	9

- (1) Both ferrimagnetic and ferromagnetic compounds allow AOS.
- (2) All the materials tend to be very thin.
- (3) Nearly all the materials,<sup>40</sup> except one sample,<sup>6</sup> have perpendicular magnetic anisotropy.
- (4) The list is dominated by rare-earth  $4f$  compounds and  $5d$  materials. Therefore, any theory that aims to explain AOS must start from the above three basic features.
- (5) There is no agreement on a unified mechanism. Proposed mechanisms tend to eliminate each other out. Any new mechanism must be conceived at least one level more microscopic and more fundamental than the existing ones.
- (6) What is not shown in the table is that the laser intensity has a narrow region to switch spins, beyond which AOS does not occur. The laser intensity is lower than that for demagnetization.

### 3. Role of Spin Angular Momentum and Spin Configuration in AOS

#### 3.1. Materials that do not switch – Iron nanoarrays

There are many more magnetic materials which do not switch their spins under laser excitation than those which do switch. Most ferromagnets only demagnetize. To understand why they do not switch, we present an example first. In 2017, Ren *et al.*<sup>41</sup> employed a group of Fe, Fe/Pt, and Fe<sub>3</sub>O<sub>4</sub> nanoarrays, with thickness of 50 nm to 200 nm. These nanoparticles have a diameter of about 50 nm, and the center-to-center distance is 100 nm. They shined a 50-fs and 800-nm laser pulse on to the samples. They found that upon laser excitation, the field-free Faraday rotation angle in Fe nanoarrays is sharply reduced, (see Fig. 2). It may appear that the sample simply demagnetizes. However, this is not the whole story. At 0 fs, the hysteresis loop has a normal rectangular shape, but around 15 fs, the signal at zero field is stronger than at nonzero field. This indicates that the spin, under joint effects of the laser field and applied magnetic field, deviates from its original direction. One sees that a diamond shape is completely formed around 55 fs (see Fig. 2), regardless of whether they employ  $\sigma^+$ ,  $\sigma^-$ , or  $\pi$  pulses.<sup>41</sup> After 150 fs, the normal rectangular shape is restored. This shows that besides the demagnetization, the spin also cants out of the sample surface, but spin switching is not observed.

In the experiment, the pump incident to the sample has fluence of  $25\mu\text{J}/\text{cm}^2$ . The probe pulse is incident at  $35^\circ$  with respect to the sample normal. The pump fluence has to be kept low to cant spins; if the pump fluence is higher, it only demagnetizes the sample without spin canting. This shows that spin canting needs much less energy. To explain this spin canting, we employ a simple theory restricted to a single site as outlined previously,<sup>42</sup> which will be explained in detail below. The model includes the kinetic and potential energy terms, both of which are expressed

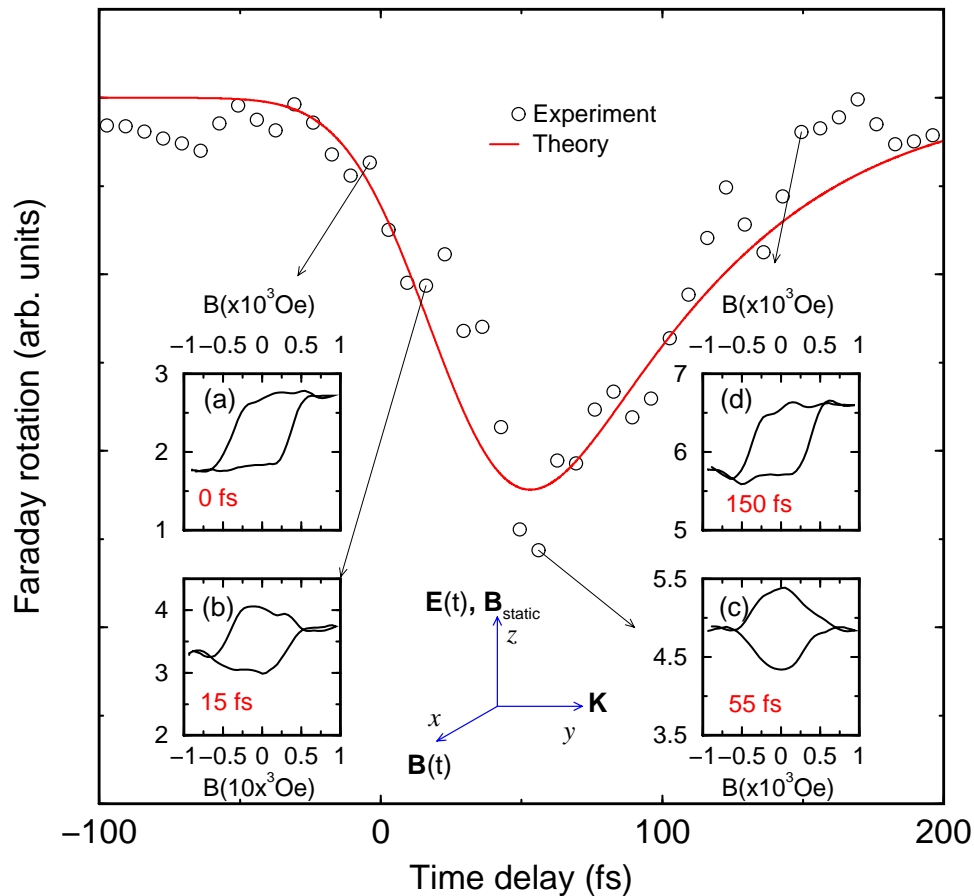


Fig. 2. Experimental Faraday rotational angle in Fe nanoarrays as a function of time delay between the pump and probe (empty circles) and theoretical spin change with time (solid line). (a)-(d) show the hysteresis loops at delays of 0, 15, 55 and 150 fs, respectively. The pump fluence is fixed at  $\sim 25 \mu\text{J}/\text{cm}^2$ . The loops were recorded by the probe beam with a photoelastic modulator (PEM) frequency. Before the arrival of pump pulses, a simple square shaped loop is observed, as expected for the easy axis. After the pump pulse excitation, the magnetization vector rotates away from the longitudinal direction, and the hysteresis loop reaches a full diamond shape at 55 fs. The loop then retrieves and recovers to the original square shape at 150 fs. Inset: Configurations of the static magnetic field  $\mathbf{B}_{\text{static}}$  and laser electric  $\mathbf{E}(t)$  and magnetic fields  $\mathbf{B}(t)$ . The laser propagates along the  $y$  axis with wavevector  $\mathbf{K}$ . Reproduced from Y. Ren, W. Lai, Z. Cevher, Y. Gong and G. P. Zhang, *Applied Physics Letters* **110**, 082404 (2017), with the permission of AIP Publishing.<sup>41</sup>

in real spaces. This allows us to compute the expectation values of the electron velocity and position. The laser field is included through a dipole term. The model is similar to the classical harmonic oscillator model. But what is different from the traditional magneto-optics formalism, is that we include a spin-orbit coupling in real space, instead of a magnetic field.<sup>42</sup> This surprisingly captures the early

switching of the spin. It was later found that the spin-orbit torque plays a role in AOS.<sup>43</sup>

The simulation uses the same laser parameters as the experimental ones, and has a single fitting parameter for the recovery of the spin. The static magnetic field and laser field directions are shown in the inset of Fig. 2. The solid line shown in Fig. 2 is our theoretical result. One can see that the theory matches the experimental results quite well. The theory shows that the spin cants out of plane and oscillates within the  $xy$  plane.<sup>41</sup> This is the first experimental verification of the model,<sup>42</sup> which is beyond the semiempirical model.<sup>6</sup> Our model further shows that regardless of spin configuration, the spin switching is not observed for in-plane magnetic anisotropy in this system. The reason is because the in-plane anisotropy is unfavorable to AOS and the spin angular momentum is too small.<sup>44</sup>

In fact, AOS was never found in any of three  $3d$  element ferromagnets, Ni, Fe and Co, and  $4f$  rare earth magnets, Gd and Tb. In these materials, even spin canting by light is rare, though canting can be induced magnetically.<sup>45</sup> Ren's study reveals an important fact that the dimensionality matters. In Ni thin films, only demagnetization is observed.<sup>4</sup> Another piece of information from Ren's work is that those nanoarrays all have in-plane magnetic anisotropy, in contrast to all the compounds listed in Table 1 which have perpendicular magnetic anisotropy (PMA). So, the next question is what the reduced dimensionality and PMA imply microscopically.

### 3.2. Impact of thickness and reduced dimension

One obvious answer is that the reduced dimensionality strengthens the perpendicular magnetic anisotropy. But this can not be the only reason for AOS, since many magnetic thin films have PMA and many do not switch spins under laser excitation. We choose two sets of experimental data from two independent groups. One is from El Hadri *et al.*<sup>46</sup> and the other is from Hebler *et al.*<sup>36</sup> They used two different samples,  $\text{Tb}_x\text{Co}_{100-x}$  and  $\text{Tb}_x\text{Fe}_{100-x}$ , respectively, with various thicknesses. We caution that when the thickness is thin, the nominal thickness may differ from the actual thickness. We see the thickness as a good gauge to test the effect of the dimensionality on AOS, so we plot the thin film thickness with the composition, where AOS or thermal demagnetization (TD) is observed. Figure 3(a) shows that AOS occurs in very thin films. If the composition of Tb ( $x$ ) is smaller, the window of thickness for AOS is narrower. As  $x$  increases, the window of thickness gets wider. The AOS-allowable thickness reaches 20 nm if  $x$  increases to 30%.  $x$  can not increase forever, since the composition of Co becomes too low to switch spins. This is probably the reason behind the peak in Fig. 3(a). A direct consequence of  $x$  is that it affects the effective spin moment for each element. If this is true, we should expect that  $\text{Tb}_x\text{Fe}_{100-x}$  allows a thicker sample for AOS. Figure 3(b) shows that it is indeed true that for a similar composition  $x$  around 30% in  $\text{Tb}_x\text{Fe}_{100-x}$ , the maximum thickness reaches 28 nm, while in  $\text{Tb}_x\text{Co}_{100-x}$ , it is only 20 nm. According to Albrecht,<sup>47</sup> for a Tb content of about 28%, AOS is even possible for TbFe films at



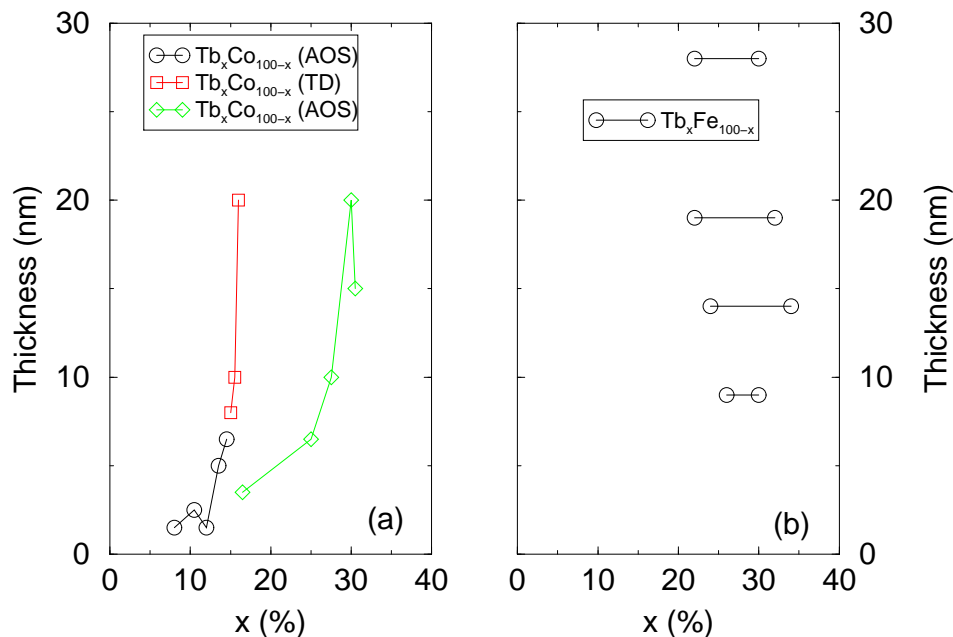


Fig. 3. Relation between thickness and composition in AOS materials. (a) TbCo-based AOS materials are normally very thin (see circles). If the thickness increases, the Tb composition  $x$  must increase (see diamonds). Otherwise, thermal demagnetization (TD) is observed (see squares). This shows the importance of the large spin moment of each constituent. The original data are from Ref. 46. (b) TbFe-based AOS alloys are also thin. But their thickness can be slightly larger than those in (a), since Fe has a larger spin moment than Co. The original data are from Ref. 36.

least as thick as 85 nm, the maximal thickness investigated. These two results seem to suggest that there is a minimum spin angular momentum which each element in these two compounds has to exceed before AOS can occur. The reduced thickness facilitates a boost of the spin moment. However, these two experimental results are not enough to make a definitive conclusion. Naturally, reduced dimensionality also affects other properties. For instance, Yuan *et al.*<sup>48</sup> showed that in Co/Pt multilayers the demagnetization field inversely depends on cobalt thickness.

### 3.3. Extracting spin angular momenta from real materials

Let us to find how large the spin angular momenta are in real samples. To extract spin moments from each element of a complex amorphous sample is highly non-trivial. Nearly all the experiments give magnetization, not spin moment. A change from magnetization to spin moment needs the volume of a sample, which is rarely given. Added to the complication is magnetization in the unit of kA/m or emu/cc (electromagnetic unit cubic centimeter).

In 2016, we found a method<sup>43</sup> which is not perfect but works reasonably

10 *Zhang, Murakami, Si, Bai, and George*

well. However, the scheme was never published formally, but it was posted on Arxiv.org.<sup>49</sup> Interestingly, a similar method was used by others.<sup>50</sup> The following material is adopted from the post with minor changes. What we do is to replace the sample volume by the unit cell volume. The unit cell of an amorphous sample is approximated by the unit cells of element constituents. Then, we use the same proportional relation to compute the spin moments of each constituent. To show how this works, we consider a rare-earth-transition metal alloy,  $R_xT_{1-x}$ , where R stands for Tb or Gd, and T stands for Fe. We ignore Co since its concentration is too low. We first compute the effective volume

$$V_{eff} = xV_R + (1-x)V_T, \quad (1)$$

where  $V_R$  and  $V_T$  are the supercell volumes of the pure elements R and T, respectively. Tb has a hcp structure, with the lattice constants  $a = 3.601\text{\AA}$  and  $c = 5.6936\text{\AA}$ ; Fe has a bcc structure with  $a = 2.8665\text{\AA}$ . Then we multiply the magnetization  $m$  for a particular element by  $V_{eff}$  to get the effective spin moment for the alloy, i.e.,  $M_{eff} = mV_{eff}$ . Since  $M_{eff}$  is in the units of  $[\text{Am}^2]$ , we convert it to the Bohr magneton  $\mu_B$ , with the conversion factor of  $0.10783 \times 10^{-3}$  (i. e.,  $10^{-3}/9.274$ ).

Szpunar and Kozarzewski<sup>51</sup> carried out extensive calculations on transition-metal and rare-earth intermetallic compounds by comparing their results with the experimental ones, and concluded that it is reasonable to assume that the average magnetic moments of the transition metals and of the rare earth metals are roughly independent of structures. Hansen and Witter<sup>5</sup> specifically tested the linear relationship between the uniaxial anisotropy constant  $K_u$  measured by the torque method and the Tb content and found the single-ion contribution of the terbium atom, so the TbFe alloy has  $K_u(\text{Temp}) = xK_u^{\text{Fe}}(\text{Temp}) + (1-x)K_u^{\text{Tb}}(\text{Temp})$ , where Temp is temperature. In the same spirit, we approximate the effective spin moment  $M_{eff}$  as

$$M_{eff} = xM_R + (1-x)M_T \equiv M_R^{eff} + M_T^{eff}, \quad (2)$$

where  $M_R$  and  $M_T$  are the spin moments of pure R and T, respectively. Here the last equation defines the effective spin moment for R and T.

However, this single equation is not enough to compute  $M_R$  and  $M_T$  since there are two unknowns for a single equation. The trick is that we use two sets of compositions,  $x_1$  and  $x_2$ , so we have two equations,

$$M_{eff}^{(1)} = x_1M_R + (1-x_1)M_T \quad (3)$$

$$M_{eff}^{(2)} = x_2M_R + (1-x_2)M_T, \quad (4)$$

where  $M_{eff}^{(1)} = m_R^{(1)}V_{eff}^{(1)}$  and  $M_{eff}^{(2)} = m_R^{(2)}V_{eff}^{(2)}$ . Here again we rely on the assumptions that  $M_R$  and  $M_T$  do not change much with composition change from  $x_1$  to  $x_2$ . When we choose  $x_1$  and  $x_2$ , we are always careful whether  $M_R$  or  $M_T$  changes sign, since experimentally the reported values are the absolute values. In addition, it is

always better to choose those  $x_1$  and  $x_2$  which have the same sign of  $M_R$  and  $M_T$ . Choosing several different pairs of  $(x_1, x_2)$  is crucial for a reliable result. Solving the above two equations, we can find  $M_R$  and  $M_T$ .

Before we compute the spin angular momentum, we check whether the computed spin moments  $M_R$  and  $M_T$  (in the units of  $\mu_B$ ) are close to their respective values of each pure element, i.e.,  $M_{\text{Gd}}^\circ = 7.63\mu_B$ ,<sup>52</sup>  $M_{\text{Tb}}^\circ = 9.34\mu_B$ , and  $M_{\text{Fe}}^\circ = 2.2\mu_B$ . If a computed spin moment ( $M_R$  and  $M_T$ ) is far off from those spin moments, this indicates that either our method or the experimental result is not reliable. Once the spin moment passes this test, we proceed to convert the spin moment to spin angular momentum.

Our method works better for Gd alloys than Tb alloys, since the former has nearly zero orbital angular momentum but the latter has a nonzero orbital angular momentum. For Gd and Fe, the orbital momentum is largely quenched. Assuming that the Lande  $g$ -factor is 2, we divide the spin moments  $M_R$  and  $M_T$  by 2 to get the spin angular momenta  $S_R$  and  $S_T$  in the unit of  $\hbar$ . To get the effective spin angular momentum, we multiply  $S_R$  and  $S_T$  with  $x$  and  $1 - x$ , respectively, i.e.,

$$S_R^{eff} = xS_R \quad (5)$$

$$S_T^{eff} = (1 - x)S_T. \quad (6)$$

It is these two effective spin angular momenta to which we apply our minimum spin angular momentum criterion (see below for details). For Tb, our results have an uncertainty since its orbital angular momentum in its alloys is unknown, although its orbital angular momentum in pure Tb metal is  $3.03\hbar$ . Table 2 shows the orbital-free spin angular momentum for 11 alloys, where we adopt a simple cubic structure for Fe since it matches the experimental values better. There are multiple rows of spin angular momenta for the same materials because there are several possible pairs of  $(x_1, x_2)$  for Eq. (4) that one can choose. For instance,  $\text{Tb}_{30}\text{Fe}_{70}$ , the composition-weighted spin angular momentum of Tb ranges between  $2.1506\hbar$  and  $1.4952\hbar$ . The variation seen in those momenta is because we choose multiple pairs of TbFe. For instance, if we choose  $\text{Tb}_{30}\text{Fe}_{70}$  and  $\text{Tb}_{29}\text{Fe}_{71}$  as a pair, we get a composition-weighted momentum; if we choose  $\text{Tb}_{30}\text{Fe}_{70}$  and  $\text{Tb}_{22}\text{Fe}_{78}$ , we get another momentum. In principle, if the magnetic properties among different compositions are independent of composition, one should find the same momentum, but this is not always the case since these materials are amorphous; different patches of samples may have different structural and magnetic properties. In the Appendix, we have provided our computer code and one example, so the reader can directly use it for his/her own research. We note that in some cases, our method can even test the accuracy of the original experimental data. However, our method does not work well for TbCo, partly because there are only two data points.<sup>32</sup>

Now, we have a table of effective spin angular momenta to work with. Table 2 shows that each constituent has a sizable spin within AOS-allowed  $x$  that is above  $0.8\hbar$  as shown next.

Table 2. Computed effective spin angular momenta for each element in GdFeCo and TbFe alloys. Multiple pairs of alloys are used to compute the effective spin angular momentum for several compounds to demonstrate the range of the change in the spin angular momentum. The sign convention of the spin angular momentum is that either Gd or Tb has a positive value, while Fe has a negative value. A simple cubic structure is adopted for Fe. Two underlined entries are two examples that are explained in the Appendix.

Alloy	$S_{\text{Gd}}^{\text{eff}}(\hbar)$	$S_{\text{Fe}}^{\text{eff}}(\hbar)$	$S_{\text{Tb}}^{\text{eff}}(\hbar)$ (orb. free)	$S_{\text{Fe}}^{\text{eff}}(\hbar)$ (orb. free)
Gd <sub>28</sub> Fe <sub>63</sub> Co <sub>9</sub>	1.3414	-1.1691	–	–
Gd <sub>26</sub> Fe <sub>64.7</sub> Co <sub>9.3</sub>	1.2456	-1.2006	–	–
Gd <sub>25</sub> Fe <sub>65.6</sub> Co <sub>9.4</sub>	1.1517	-1.1777	–	–
Gd <sub>24</sub> Fe <sub>66.5</sub> Co <sub>9.5</sub>	1.2262	-1.3017	–	–
Gd <sub>24</sub> Fe <sub>66.5</sub> Co <sub>9.5</sub>	1.0867	-1.0113	–	–
Gd <sub>22</sub> Fe <sub>68.2</sub> Co <sub>9.8</sub>	1.1241	-1.3350	–	–
Gd <sub>22</sub> Fe <sub>68.2</sub> Co <sub>9.8</sub>	1.0135	-1.2244	–	–
Gd <sub>22</sub> Fe <sub>68.2</sub> Co <sub>9.8</sub>	0.9846	-0.7737	–	–
Gd <sub>22</sub> Fe <sub>74.6</sub> Co <sub>3.4</sub>	0.9846	-0.8463	–	–
<u>Tb<sub>30</sub>Fe<sub>70</sub></u>	–	–	2.1506	-1.8385
Tb <sub>30</sub> Fe <sub>70</sub>	–	–	1.7594	-1.4473
Tb <sub>30</sub> Fe <sub>70</sub>	–	–	1.4952	-1.1831
Tb <sub>30</sub> Fe <sub>70</sub>	–	–	1.4698	-1.1577
<u>Tb<sub>29</sub>Fe<sub>71</sub></u>	–	–	2.0789	-1.8648
Tb <sub>27</sub> Fe <sub>73</sub>	–	–	1.5835	-1.5093
Tb <sub>27</sub> Fe <sub>73</sub>	–	–	1.1867	-1.1125
Tb <sub>24</sub> Fe <sub>76</sub>	–	–	1.2641	-1.3452
Tb <sub>24</sub> Fe <sub>76</sub>	–	–	1.1758	-1.2569
Tb <sub>22</sub> Fe <sub>78</sub>	–	–	1.2789	-1.5007
Tb <sub>22</sub> Fe <sub>78</sub>	–	–	1.1587	-1.3806
Tb <sub>22</sub> Fe <sub>78</sub>	–	–	1.0965	-1.3183
Tb <sub>22</sub> Fe <sub>78</sub>	–	–	0.9669	-1.1887

### 3.4. Dynamical simulation

Different from the magnetic field-driven spin reversal, AOS relies on a laser field to flip spin from one direction to another. However, to describe such a process has been a big challenge. Most simulations have been phenomenological,<sup>6</sup> where laser fields are treated as an effective magnetic field.<sup>13</sup> Ostler *et al.*<sup>6</sup> and Mentink *et al.*<sup>53</sup> showed that in GdFeCo, HID-AOS and HD-AOS depend on the laser intensity (electric field squared), not the field helicity. As shown in our recent study,<sup>54</sup> caution must be taken if the system has two spin sublattices. Because the laser field is only active for one sublattice, two sublattices are present and they separately allow the laser field of either helicity to switch spin, so the final results appear to the reader that AOS only depends on the laser intensity. If one only has one spin orientation such as in CoPt ultrathin films, the impact of the laser field, not just the laser

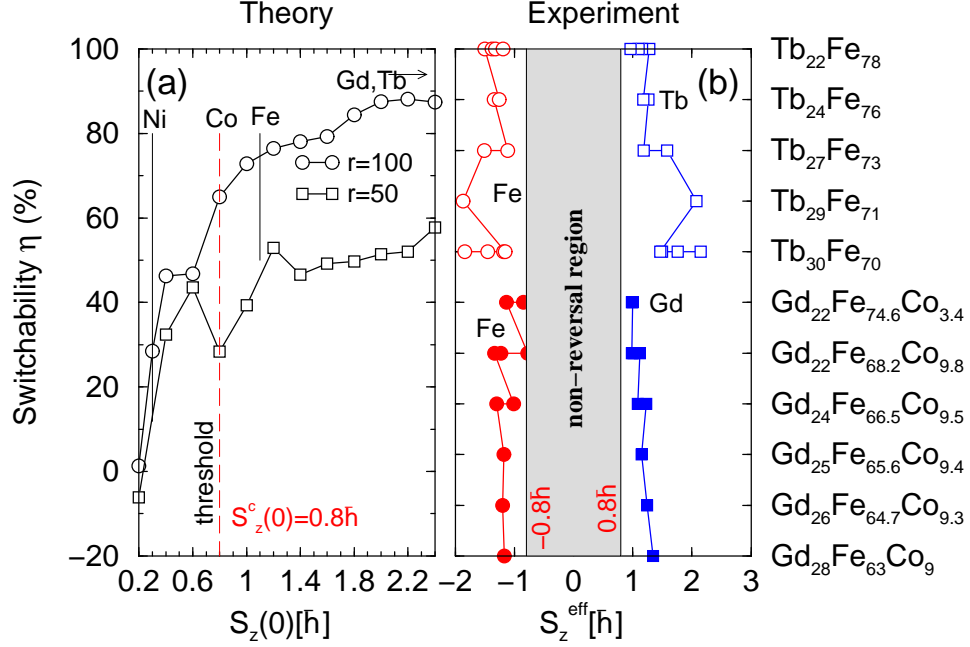


Fig. 4. (a) Spin switchability versus the initial spin angular momentum  $S_z(0)$  at the respective optimal laser field amplitudes.<sup>43</sup> The empty circles and boxes refer to the results with  $r = 100$  and  $r = 50$ , respectively. The long-dashed line denotes the critical spin  $S_z^c$ . Two thin vertical lines represent the spins for Ni and Fe. Co is on the border line, while Gd and Tb are way above  $S_z^c$ . The arrow on the top right refers to the fact that Gd and Tb have a much higher spin angular momentum. (b) Computed experimental effective spin angular momentum for each element in 11 GdFeCo and TbFe alloys.<sup>32</sup> Without exception, all elements have spin larger than  $S_z^c$ . Used with permission from EPL.

intensity, appears.

In our view, the key to AOS theory is to include the microscopic interaction between laser pulses and systems. In 2016, we introduced a new formalism that couples laser excitation to spin through spin-orbit coupling, while the spin-spin interaction is described by the Heisenberg exchange Hamiltonian, and electrons move inside a harmonic potential.<sup>42</sup> This model, though simple, overcomes traditional difficulties that laser excitation and spin dynamics are treated as two separate entities. Specifically, the Hamiltonian is<sup>42,43</sup>

$$H = \sum_i \left[ \frac{\mathbf{p}_i^2}{2m} + V(\mathbf{r}_i) + \lambda \mathbf{L}_i \cdot \mathbf{S}_i - e\mathbf{E}(\mathbf{r}, t) \cdot \mathbf{r}_i \right] - \sum_{ij} J_{ex} \mathbf{S}_i \cdot \mathbf{S}_j. \quad (7)$$

The summation is over all the lattice sites. Here, the first term is the kinetic energy operator of the electron; the second term is the harmonic potential energy operator with system frequency  $\Omega$ ;  $\lambda$  is the spin-orbit coupling in units of  $\text{eV}/\hbar^2$ ;  $\mathbf{L}$  and  $\mathbf{S}$  are the orbital and spin angular momenta in units of  $\hbar$ , respectively; and  $\mathbf{p}$  and  $\mathbf{r}$

are the momentum and position operators of the electron, respectively. Note that  $\mathbf{L}$  is computed from  $\mathbf{L} = \mathbf{r} \times \mathbf{p}$ , and there is no need to set up a different equation for it. The last term is the exchange interaction, and  $J_{ex}$  is the exchange integral in units of  $\text{eV}/\hbar^2$ . Such a Hamiltonian contains the necessary ingredients for AOS. To our knowledge, this is the only model that can generate spin reversal without introducing a semiempirical effective magnetic field.

To demonstrate the power of this model, Figure 4(a) shows the theoretical result for the switchability  $\eta$  as a function of spin angular momentum  $S_z$  in a ferromagnetic slab for two radii of the laser radiation: one is the uniform radiation over the entire sample, and the other is half the uniform radius.<sup>43</sup> The spin switchability is defined as  $\eta = \frac{S_z^f}{S_z(0)} \times 100\%$ , where  $S_z^f$  is the final spin angular momentum. It is clear that  $\eta$  increases with  $S_z$ . In order to realize AOS, there is a threshold value for the spin momentum,  $S_z^c = 0.8 \pm 0.2\hbar$ , that the material spin momentum has to exceed. For instance, pure Ni can not exhibit AOS. Co is on the threshold. As we noted before,<sup>43</sup> Co-Pt granular samples<sup>55</sup> have an effective spin magnetic moment per  $3d$  hole of  $0.77 \mu_B$ ; since there are 2.49-2.62 holes, the spin angular momentum is  $0.96\hbar$ , satisfying this criterion.

What is even more interesting is that when we reduce the laser spot size, the switch becomes more difficult. It is truly gratifying that we predicted this result before the latest experimental results were reported.<sup>9</sup>

We want to make connection with the above found spin angular momentum. Figure 4(b) shows a comparison with all 11 rare-earth transition-metal ferrimagnets. These ferrimagnets show AOS. It is remarkable that all the elements have spin angular momenta exceeding the threshold value of  $0.8\hbar$ . To understand the window of concentration  $x$ , Figure 5 plots the spin moment as a function of the Gd concentration  $x$ . Two horizontal dashed lines set the spin threshold for each element. The rectangular box delineates the window for all-optical switching. The agreement between experiment and theory gives confidence that the model works reasonably well.

#### 4. Simple Theory for All-Optical Switching

Despite a decade of investigation, our understanding is still very limited. As discussed above, the majority of theoretical research has been phenomenological.<sup>13</sup> This calls for a systematic experimental investigation by tuning both system- and laser-specific parameters. Before one can pin down the origin of AOS, it is necessary to develop a many-to-one correspondence between the proposed mechanisms (see Table 1) and more fundamental interactions. However, the majority of the proposed mechanisms are very difficult to attribute to a single interaction. We speculate that the requirement of compensation points can be mapped to the requirement of a sizable spin moment, while the domain size criterion could be a result associated with radiation size as shown in our recent study<sup>56</sup> and the Vomir *et al.* observation.<sup>9</sup>

By contrast, theoretically the inverse Faraday effect is more mature and has an

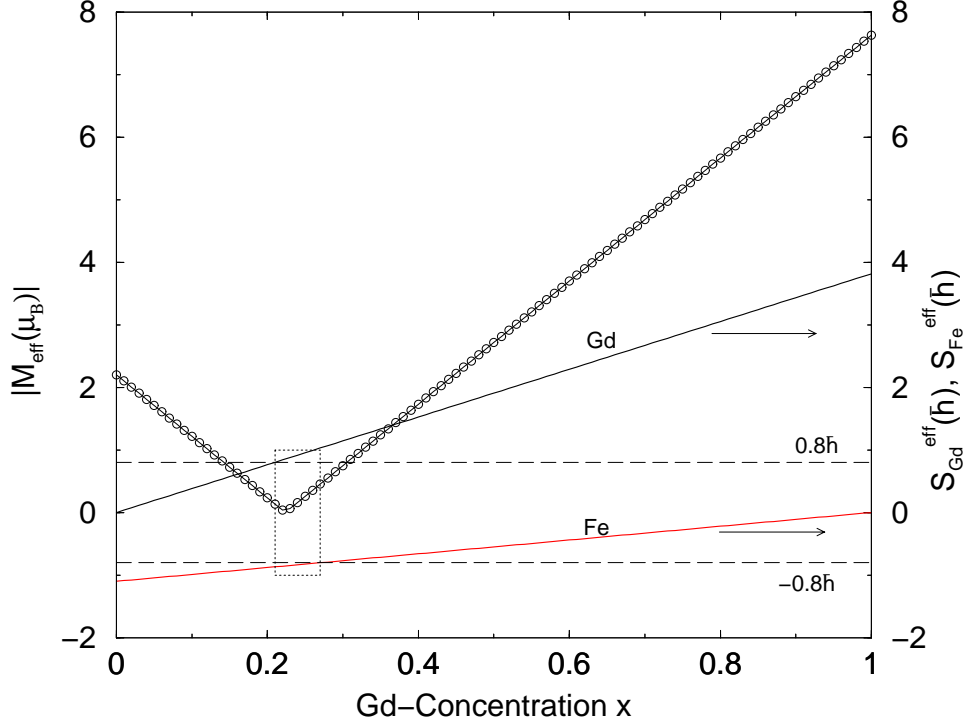


Fig. 5. Effective spin moment change as a function of the Gd concentration  $x$  (circles). The two solid lines represent the effective spin angular momenta for Gd and Fe (using the right axis). The two horizontal dashed lines denote the predicted critical spin angular momenta ( $\pm 0.8\hbar$ ). The dotted line box highlights the narrow region of the Gd concentration where spin angular momentum satisfies our criterion and the spin reversal occurs.

existing theory developed for a nonabsorbing medium.<sup>57</sup> According to Shen,<sup>58</sup> the optical field-induced magnetization is

$$\Delta M_F = i \frac{\partial \chi_{xy}}{\partial H_0} (|E_+|^2 - |E_-|^2), \quad (8)$$

where  $H_0$  is the static magnetic field and  $\chi_{xy}$  is the susceptibility. Interestingly, this expression is different from the commonly used one with the field product  $\mathbf{E} \times \mathbf{E}$ . Note that Shen considered a nonabsorbing medium. Here  $E_+$  and  $E_-$  are  $(E_x - iE_y)/\sqrt{2}$  and  $(E_x + iE_y)/\sqrt{2}$ , respectively.<sup>57</sup> For linearly polarized light,  $E_+ = E_-$ , so  $\Delta M_F = 0$ ; for circularly polarized light,  $\Delta M_F$  is nonzero and changes signs from the left-circularly polarized light to the right one.  $\chi_{xy}$ 's frequency dependence is not considered.<sup>57</sup> To apply the above equation to an absorbing material, we use our susceptibility<sup>42,13</sup> for a single site. Our model<sup>42</sup> does not have an external field, but has a spin-orbit coupling (see Eq. (7)), so the spin angular momentum plays the same role as the magnetic field. Note that in the SI unit system, the linear

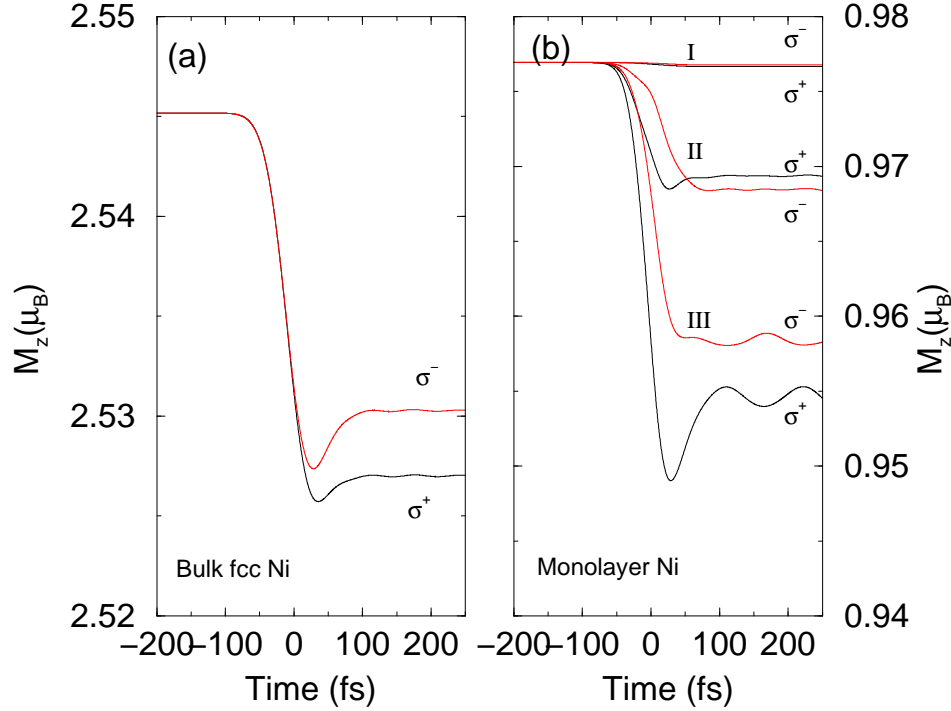


Fig. 6. (a) Spin moment change as a function of time in fcc Ni for the left ( $\sigma^-$ ) and right ( $\sigma^+$ ) circularly polarized light. The laser pulse duration is  $\tau = 60$  fs, the photon energy is  $\hbar\omega = 2$  eV, and the field amplitude is  $A_0 = 0.0099$  Vfs/Å. (b) Spin moment change as a function of time in monolayer Ni for left ( $\sigma^-$ ) and right ( $\sigma^+$ ) circularly polarized light. We choose three sets of laser parameters. I:  $\tau = 48$  fs,  $\hbar\omega = 1.6$  eV and  $A_0 = 0.0030$  Vfs/Å; II:  $\tau = 48$  fs,  $\hbar\omega = 1.6$  eV and  $A_0 = 0.030$  Vfs/Å; III:  $\tau = 48$  fs,  $\hbar\omega = 1.55$  eV and  $A_0 = 0.030$  Vfs/Å.

susceptibility  $\chi_{xy}^{(1)}$  has no unit. We take the derivative of  $\chi_{xy}^{(1)}$  with respect to  $S_z$ .  $\chi_{xy}^{(1)}$  has  $S_z$  in its numerator and denominator, so the derivative is complicated. For simplicity, we only include the derivative from the numerator. We have the magnetization change

$$\Delta M_F \propto \frac{Ne^2}{\epsilon_0 m} \frac{2\lambda\omega}{(\Omega^2 - \omega^2 - \lambda^2 S_z^2)^2 - (2\lambda S_z \omega)^2} (|E_+|^2 - |E_-|^2), \quad (9)$$

where  $\lambda$  is the spin-orbit coupling and  $S_z$  is the spin angular momentum. Other variables can be found in our prior paper.<sup>42</sup> This relation highlights the importance of the spin-orbit coupling and reveals how circularly polarized light may affect spins.

The above results are reproduced in our first-principles calculation. We carry out a lengthy calculation using the time-dependent Liouville density functional theory<sup>56</sup> for both bulk fcc Ni and monolayer Ni. We employ both  $\sigma^+$  and  $\sigma^-$ . We choose a 60-fs laser pulse with photon energy 2 eV and vector potential amplitude 0.009 Vfs/Å. Figure 6(a) shows that the laser helicity does affect the spin moment



change.<sup>15</sup> We see that  $\sigma^+$  can demagnetize Ni more than  $\sigma^-$ . In the simulation, we adopt a simple cubic structure for fcc Ni, so there are four Ni atoms in our cell. Figure 6(b) shows the results for a Ni(001) monolayer for three sets of laser parameters, labeled by I, II and III. For I, we use  $\tau = 48$  fs,  $\hbar\omega = 1.6$  eV and  $A_0 = 0.0030$  Vfs/Å. We see that under such a weak laser pulse the demagnetization is very small. However, the difference in spin moment between  $\sigma^+$  and  $\sigma^-$  excitation is also visible. Set II shows an increase in the laser field amplitude to  $\tau = 48$  fs,  $\hbar\omega = 1.6$  eV and  $A_0 = 0.030$  Vfs/Å. We find that different helicity induces different demagnetization. Even the demagnetization time is different, 27 fs for  $\sigma^+$  and 84 fs for  $\sigma^-$ . It is not always true that one kind of helicity dominates all the time. We also investigate how the photon energy affects the demagnetization. We decrease the photon energy to set III with the laser parameters  $\tau = 48$  fs,  $\hbar\omega = 1.55$  eV and  $A_0 = 0.030$  Vfs/Å. Figure 6(b) shows that in comparison with set II, the monolayer demagnetizes more for the same laser helicity as we decrease the photon energy. In addition, there is a strong oscillation in the spin moment. In this case,  $\sigma^+$  induces a more pronounced change.

While the above analytic and numerical results are insightful in themselves, they miss some crucial experimental and numerical findings. For instance, numerically we find that linearly polarized light can switch spins as well if the laser field amplitude becomes stronger,<sup>42,43</sup> but Eq. (9) gives zero for linearly polarized light. This highlights that this analytic expression, which is obtained under perturbation theory, does not catch the actual spin reversal completely. Our first-principles result only shows the demagnetization, not switching. The only way that we can get true spin reversal is to use the Hamiltonian of Eq. (7). We find that the actual switching may result from the spin-orbit torque,<sup>13</sup>

$$\tau = \lambda \mathbf{L} \times \mathbf{S}, \quad (10)$$

where  $\mathbf{L}$  is the orbital angular momentum. This was first tested by Ren *et al.* experimentally.<sup>41</sup>

Recently we constructed a phase diagram, which is reproduced in Fig. 7.<sup>54</sup> We suggest that all the AOS materials should be classified into three categories: ferromagnetic, weak and strong ferrimagnetic. In both ferromagnets and weak ferrimagnets, only one spin orientation is present or dominant, and switching is helicity-dependent. For strong ferrimagnets, since both sublattices have a strong magnetic moment, circularly polarized light with different helicities can switch spins. This is potentially useful for future device design.

## 5. Importance of Perpendicular Magnetic Anisotropy: Emergence of Orbital Angular Momentum

From the above discussion, it should be clear that one needs a large spin moment for each constituent in a compound in order to switch spins optically. However, if this is the sole criterion, then the strongest man-made magnet Nd<sub>2</sub>Fe<sub>14</sub>B would be

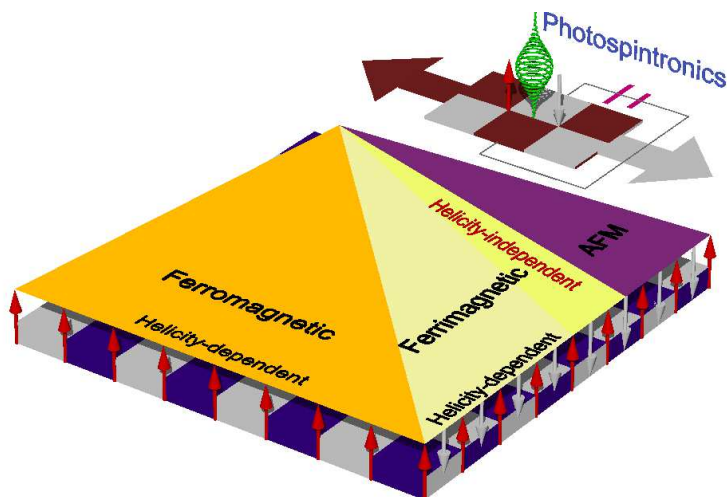


Fig. 7. Phase diagram of AOS. Switchings in ferromagnetic (orange triangle) and weak ferromagnetic materials (light yellow triangle) are always helicity-dependent. Helicity-independent switching (yellow triangle) occurs in a narrow region when the sublattice spins approach the antiferromagnetic limit.<sup>54</sup>

the best candidate for AOS. However, this does not happen. One crucial element among all the six common themes is perpendicular magnetic anisotropy (PMA).

We decide to first examine the universal presence of perpendicular magnetic anisotropy (PMA) in nearly all the AOS materials. From our prior investigation,<sup>44</sup> we find that PMA has an unparalleled advantage over other spin configurations. The presence of PMA demands a nonzero orbital angular momentum. It is well known that in thin films, the surface contribution, which favors PMA, becomes larger. However, in solids the orbital angular momentum is largely quenched by the crystal field. This statement is based on the symmetry argument. If two spherical harmonics  $Y_{lm}$  and  $Y_{l\bar{m}}$  in a Bloch state have the same weight, then the summation of the orbital angular momentum expectation value  $\langle Y_{lm} | l_z | Y_{lm} \rangle + \langle Y_{l\bar{m}} | l_z | Y_{l\bar{m}} \rangle$  is zero, where  $l_z$  is the orbital angular momentum operator along the  $z$  axis. With the presence of spin-orbit coupling, the equivalency of the two harmonics breaks down. The level of breakdown depends on the strength of the spin-orbit coupling. If we go back to Table 1, we notice that rare-earth and  $5d$  elements are present in all the materials. They are known for their strong spin-orbit coupling. This implies a sizable orbital momentum present in those compounds.

However, one often argues that since Gd atom has a half-filled  $4f$  shell, its orbital angular momentum is zero. However, this is no longer the case in solids. Even in pure bulk Gd, the orbital momentum is nonzero. We found<sup>54</sup> that hcp Gd has (0.00002, -

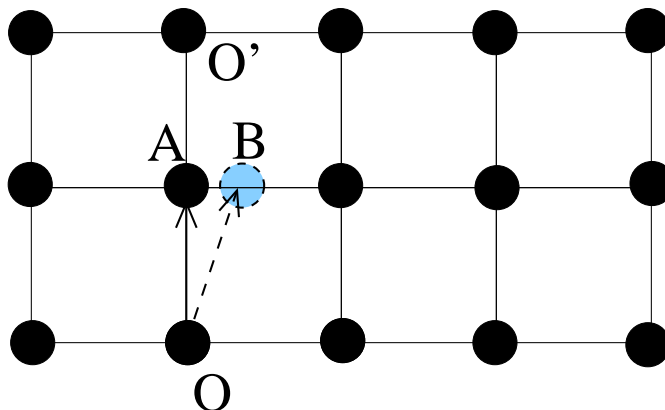


Fig. 8. Orbital angular momentum of lattice vibration in solids is difficult to define. The electron interacts with the lattice mainly through the energy exchange, instead of momentum exchange.

0.00006, 0.12166) $\mu_B$ , which is larger than that in Ni. Only if we include the Hubbard  $U$  term, can we quench it to nearly zero (-0.00006 0.00007, 0.01716) $\mu_B$ , where we use  $U = 0.4926\text{Ry}$  and  $J = 0.051\text{Ry}$ . These  $+U$  treatments rectify correlation effects in the ground state and do not change spin moments (compare 7.55298 $\mu_B$  with  $+U$  with 7.44249 $\mu_B$  without  $+U$ ), but worsen other properties, in particular excitation processes, as shown recently.<sup>54</sup> The orbital angular momentum is one of those properties for which the GGA+ $U$  treatment does not work. Jang *et al.*<sup>59</sup> recently demonstrated the existence of orbital ordering in  $\text{GdB}_4$ . Gd loses three  $5d$  electrons to B, so it becomes  $\text{Gd}^{3+}$  with its  $4f$  orbital half-filled. They found the orbital order is strongly coupled with the antiferromagnetic spin order. This matches the scenario in  $\text{GdFeCo}$ , where antiferromagnetic ordering is also present. Therefore, there is no contradiction regarding the importance of orbital angular momentum and the presence of spin-orbit coupling.

Different from the ground-state property, the orbital angular momentum can be enhanced during laser excitation, during which the laser helicity information is encoded. In other words, the electron orbital angular momentum stores the helicity information. This information can not be easily erased because the coupling between electron and lattice subsystems is through energy exchange. The lattice orbital angular momentum change, i.e., the lattice displacement  $\Delta\mathbf{R}_{\text{lattice}} \times$  the lattice momentum  $\mathbf{P}_{\text{lattice}}$ , is tiny, because  $\Delta\mathbf{R}_{\text{lattice}}$  and  $\mathbf{P}_{\text{lattice}}$  are mostly along the same direction. In fact, in a one-dimensional system, the orbital angular momentum of the lattice is always zero, since the position and momentum of the lattice are always in the same or in opposite directions. Caution must be taken for 2- and 3-dimensional systems when one tries to define the angular momentum for a lattice. The orbital angular momentum of an atom depends on the reference point and, if not treated properly, it becomes ambiguous.

In Fig. 8, we show an example, where we treat the motion of atoms classically.

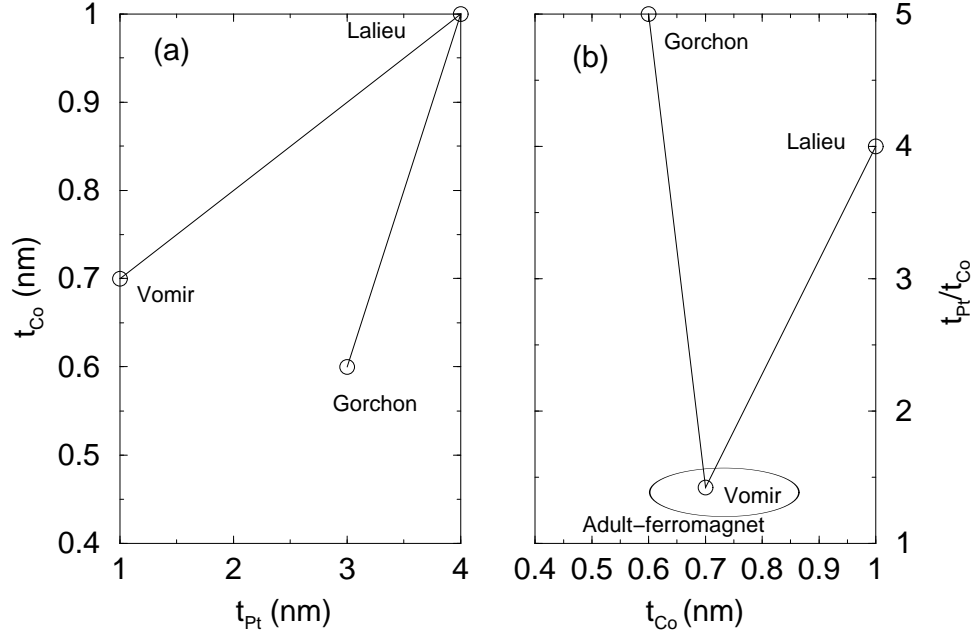


Fig. 9. Importance of layer thickness on single-shot spin switching. (a) Co layer thickness  $t_{Co}$  versus Pt thickness  $t_{Pt}$  for three experiments. (b) Ratio  $t_{Pt}/t_{Co}$  as a function of  $t_{Co}$ .

Suppose that the equilibrium position of an atom in a square lattice is at  $A$ . It linearly moves to  $B$  with a certain velocity. Such a linear motion should have zero angular momentum. However, if we choose a reference point at  $O$ , then the angular momentum is nonzero. If we choose  $O'$  as the reference point, then the angular momentum changes sign. Besides, in general, atoms in a lattice experience a crystal potential that is translationally invariant, and do not orbit. This is different from molecular crystals, such as  $C_{60}$  solids, where  $C_{60}$  spins rapidly at room temperature. For this reason, the traditional solid state theory does not invoke the orbital angular momentum transfer between electrons and lattices. The electron-phonon interaction relies on the energy transfer, where the phonon frequency is renormalized.

## 6. Path to Single-Shot Switching in Ferromagnets

Up to now, single-shot spin switching is dominated by a single material, ferrimagnet GdFeCo, which can be driven optically or electrically.<sup>60</sup> Many newly discovered materials<sup>30</sup> do not have this property. This will certainly limit future applications, as the majority of materials used for magnetic storage are ferromagnetic. Fortunately, recent studies show there are at least three experiments<sup>7,8,9</sup> that allow single-shot switching in ferromagnets. Two of them still rely on Gd and GdFeCo, which will be called rare-earth-assisted ferromagnets, or RE-parenting ferromag-

nets. Only one is independent, an adult-ferromagnet. All of the samples are Co/Pt ultrathin layers. While it is really premature to make sense out of a limited set of data, we wonder what makes Co/Pt so unique in this aspect. It is also interesting to note that the same material is used for spin transport.<sup>61</sup>

These experiments do not provide the detailed structure characterization and magnetic properties, except that all of them are found to have PMA. Figure 9(a) plots the thickness of a Co layer versus that of a Pt layer. We notice again that these films are extremely thin, so the surface contribution dominates. We caution again that within such a thickness, the nominal thickness may differ from the actual one. There is no clear trend among those three experiments. But it is known that the reduced dimensionality and imperfections affect PMA greatly.<sup>62</sup> The interfacial effects affect magnetic relaxations in Co/Pt multilayers.<sup>48</sup> In addition, very large domain wall velocities were found.<sup>63</sup> Atoms across the interface may segregate into different regions in nanoparticles.<sup>64</sup> The presence of PMA further indicates the presence of orbital angular momentum.<sup>65</sup> It also matters that the arrangement of atoms across the interface affects the magnetic properties. One can see this from the experiments too. Figure 9(b) plots the thickness ratio versus the Co layer thickness. The data of Vomir *et al.*<sup>9</sup> has the smallest ratio. We wonder whether this makes their sample as the only one sample for a single-shot AOS. In addition, the fact that Vomir *et al.*<sup>9</sup> obtained AOS at a much longer time indicates the damping of magnetization must be very small. This matches our expectation. Since the spin-orbit torque and spin damping result from the same spin-orbit coupling, a reduced spin-orbit coupling must have a longer switching time. Recent theoretical studies at Co/Pt interfaces reveal additional information about the Dzyaloshinskii-Moriya interaction at disordered interfaces.<sup>66</sup>

## 7. Conclusions

It is an exciting time to investigate all-optical spin switching. Progress has been very impressive. It is generally agreed that the microscopic picture of AOS is complex. AOS becomes strongly material-dependent, but what material's properties the actual dependence depends on is unclear. There are many cases where opposite situations appear simultaneously. Therefore, how to unify different fractions of underlying mechanisms has dominated much of the latest research. Yet, the theory is mostly phenomenological and far from perfect. The irony is that if one carries out a first-principles calculation for a ferromagnet, the effective switching field is tiny, and the laser simply can not switch spins. A stronger laser only demagnetizes a sample, but does not switch the spin direction. The origin of the theoretical failure is also unknown. There is a great need to construct a minimal model, without introducing an effective magnetic field, to simulate AOS. This could be helpful to understand how magnetic domains affect the switching. What we miss is the structure characterization of samples. We believe with additional experimental and theoretical investigations that AOS can be put into practical usage.<sup>67,68</sup>

22 *Zhang, Murakami, Si, Bai, and George*

### Acknowledgments

We greatly appreciate Dr. Jeff Bokor (Berkeley, US) for reviewing our paper with helpful comments and remarks on the computer clock frequency. We greatly benefited from the first two references that he provided in the first paragraph of this paper. We would like to thank Dr. Theo Rasing for reviewing our draft. Both Drs. Bokor and Rasing noted that AOS could occur in samples with in-plane magnetic anisotropy. We are extremely grateful to Dr. Manfred Albrecht (Ausburg, Germany) who has thoroughly examined our paper and provided helpful suggestions. Some of the changes are directly adopted from his comments. To support the open code initiative, we attach our computing code. The spin switching code will be presented in a book that we are completing.

This work was supported by the U.S. Department of Energy under Contract No. DE-FG02-06ER46304. M. S. Si was supported by the NSFC of China under No. 11874189. Part of the work was done on Indiana State University's quantum cluster and high-performance computers. The research used resources of the National Energy Research Scientific Computing Center, which is supported by the Office of Science of the U.S. Department of Energy under Contract No. DE-AC02-05CH11231. We would like to thank Anthony Froehlich for assistance with the figures.

### Appendix A. Computer codes for spin angular momentum in amorphous materials

! The following code was written by Guoping Zhang, January 2016 at  
! Indiana State University, Terre Haute, IN 47809, U.S.A.

! The code development was supported by U. S. Department of Energy under  
! Contract No. DE-FG02-06ER46304.

! This code allows one to compute spin angular momenta for amorphous  
! materials.

! Anyone can freely share this code. But please keep the headings.  
! Copyrighted by Guoping Zhang.

```

    implicit double precision(a-z)
    character *15 sample(2)
    character *2 element(2)
    double precision percent(2,2),magnet(2)
    integer i
!   spin: the spin for each element
!   spin_eff: the effective spin which is computed by the spin x percent
    double precision spin(2),spin_eff(2,2),spin_hbar(2,2)

```

```

double precision vol_(2)

! this is Terbium lattice constant. I only use Terbium bulk for all
! alloys.
! ml=3.03d0 ! M_l for Terbium.
a=360.1d0*1d-2
b=a
c=569.36d-2
vol_tb=a**2*c*dsqrt(3d0)/2d0
vol_fe=2.8665d0**3!/2d0
vol_co=(2.5071d0)**2*4.0695d0*dsqrt(3d0)/2d0
vol_gd=(3.636d0)**2*5.7826*dsqrt(3d0)/2d0
write(*,*)vol_tb,vol_fe,vol_co,vol_gd
open(2,file='output.data')
! write(2,*)'\hline'
open(1,file='input.data')
read(1,*)

111 read(1,*,end=110)sample(1),percent(1,1),percent(2,1),element(1)
$      ,element(2),magnet(1)

read(1,*)sample(2),percent(1,2),percent(2,2),element(1),element(2)
$      ,magnet(2)

do i=1,2
  vol_(i)=0d0
  write(*,*)i,vol_(i)
  write(*,*)i,element(i)
  if(element(i).eq.'gd')vol_(i)=vol_gd
  if(element(i).eq.'tb')vol_(i)=vol_tb
  if(element(i).eq.'fe')vol_(i)=vol_fe
  if(element(i).eq.'co')vol_(i)=vol_co
enddo

do i=1,2
  write(*,*)i,vol_(i)
enddo
! stop

call treat(sample,magnet,vol_,percent,spin,spin_eff,spin_hbar)

write(*,*)sample(1),percent(1,1),percent(2,1),element(1)
$      ,',',element(2),magnet(1)

```

24 *Zhang, Murakami, Si, Bai, and George*

```

write(*,*)sample(2),percent(1,2),percent(2,2),element(1)
$      ,'      ',element(2),magnet(2)
write(*,302)element(1),spin(1),'[uB]'
write(*,302)element(2),spin(2),'[uB]'

write(2,3021)element(1),'&',spin(1),'$\mu_{B}$','&','--&','\\'
write(2,3021)element(2),'&',spin(2),'$\mu_{B}$','&','--&','\\'

3021 format(1x,2a,f10.4,4a)

302  format(1x,a,f10.4,a)
do i=1,2
    write(*,*)sample(i),spin_eff(1,i),spin_eff(2,i),'[uB]'
    write(*,*)sample(i),spin_hbar(1,i),spin_hbar(2,i),'[hbar]'
3022  format(1x,3a,f10.4,a,f10.4,a)
    write(2,3022)sample(i),'&','&',spin_hbar(1,i),'$\hbar$&'
$      ,spin_hbar(2,i),'$\hbar$ \\'
    enddo
write(2,*)'\hline'
goto 111
110  close(1)
close(2)

stop
end
subroutine treat(sampl,magnet,vol,percent,spin,spin_eff,spin_hbar)
!   implicit double precision (a-h,o-z)
implicit none
integer i,j
!   INPUT
character *15 sampl(2)
!   percent: concentration for compound 1 percent(*,1)
double precision vol(2),percent(2,2),magnet(2)
double precision to_uB
!   output
!   spin: the spin for each element
!   spin_eff: the effective spin which is computed by the spin x percent
double precision spin(2),spin_eff(2,2),spin_hbar(2,2)

!   ax+by=s for compound (1).
!   s: the magnetization for compound (1)
!   a: percentage of element 1 = x1 in Eq. (3). For Gd_xFe_yCo, a=x

```



```

!   b: percentage of element 2 = (1-x1) in Eq. (3). For GdxFeyCo, b=y
!   x: MR in eq. (3)
!   y: MT in eq. (3)

!   cx+dy=t for compound (2)
!   t: the magnetization for compound (2)
!   c,d have the same meaning as a and b, except for compound (2)
!   x,y: see above
double precision a,b,c,d,s,t,x,y,volume

to_uB=1d-3/9.274d0      !this converts kA/m to u_B
! ax+by=s; cx+dy=t

!   this is for compound 1
a=percent(1,1)          !element 1
b=percent(2,1)          !element 2
!   volume is effective cell volume in unit of Angstrom cubic
volume=a*vol(1)+b*vol(2)
!   convert magnetization to magnetic moment, then convert to u_B
s=magnet(1)*volume*to_uB

!   this is for compound 2
c=percent(1,2)
d=percent(2,2)
volume=c*vol(1)+d*vol(2)
!   convert magnetization to magnetic moment, then convert to u_B
t=magnet(2)*volume*to_uB

!   the following is the element's spin moment in unit of u_B
y=(a*t-c*s)/(a*d-c*b)
x=(s-b*y)/a

spin(1)=x
spin(2)=y

!   effective spin for compound 1
spin_eff(1,1)=spin(1)*a  !element 1
spin_eff(2,1)=spin(2)*b  !element 2

!   effective spin for compound 2
spin_eff(1,2)=spin(1)*c  !element 1
spin_eff(2,2)=spin(2)*d  !element 2

```

26 *Zhang, Murakami, Si, Bai, and George*

```

!      convert from uB to hbar, for zero orbital angular momentum, the
!      conversion factor is 2, but if the element has a nonzero orbital
!      angularl moment. The conversion needs some caution.

      do i=1,2
        do j=1,2
          spin_hbar(i,j)=spin_eff(i,j)/2d0
        enddo
      enddo
    end
  end

```

## Appendix B. Sample input files

This file is called `input.data`. The experimental remanence is from the paper by Hassdenteufel *et al.*<sup>32</sup>

```

#compound  percentages  elements  remanent (kA/m)
Tb30Fe70----- 0.30 0.70  tb fe    162.3d0
Tb29Fe71----- 0.29 0.71  tb fe    112.64d0

```

## Appendix C. Sample output file

This file is called `output.data`.

```

tb&   14.3375$\mu_{B}$&--&\\
fe&   -5.2529$\mu_{B}$&--&\\
Tb30Fe70-----&&   2.1506$\hbar$&   -1.8385$\hbar$ \\
Tb29Fe71-----&&   2.0789$\hbar$&   -1.8648$\hbar$ \\
\hline

```

The above results are highlighted in Table 2. See the first line starting with  $\text{Tb}_{30}\text{Fe}_{70}$  and the line starting with  $\text{Tb}_{29}\text{Fe}_{71}$ .

## References

1. T. N. Theis and P. M. Solomon, It’s time to reinvent the transistor! *Science* **327**, 1600 (2010).
2. T. N. Theis and P. M. Solomon, In quest of the “next switch”: Prospects for greatly reduced power dissipation in a successor to the silicon field-effect transistor, *Proc. IEEE* **98**, 2005 (2010).
3. C. D. Stanciu, F. Hansteen, A. V. Kimel, A. Kirilyuk, A. Tsukamoto, A. Itoh, and Th. Rasing, All-optical magnetic recording with circularly polarized light, *Phys. Rev. Lett.* **99**, 047601 (2007).
4. E. Beaurepaire, J. C. Merle, A. Daunois, and J.-Y. Bigot, Ultrafast spin dynamics in ferromagnetic nickel, *Phys. Rev. Lett.* **76**, 4250 (1996).
5. P. Hansen and K. Witter, The role of the compensation temperature in thermomagnetic switching, *IEEE Trans. Magn.* **24**, 2317 (1988).

6. T. A. Ostler, J. Barker, R. F. L. Evans, R. W. Chantrell, U. Atxitia, O. Chubykalo-Fesenko, S. El Moussaoui, L. Le Guyader, E. Mengotti, L. J. Heyderman, F. Nolting, A. Tsukamoto, A. Itoh, D. Afanasiev, B. A. Ivanov, A. M. Kalashnikova, K. Vahaplar, J. Mentink, A. Kirilyuk, Th. Rasing, and A. V. Kimel, Ultrafast heating as a sufficient stimulus for magnetization reversal in a ferrimagnet, *Nat. Commun.* **3**, 666 (2012).
7. M. L. M. Lalieu, M. J. G. Peeters, S. R. R. Haenen, R. Lavrijsen, and B. Koopmans, Deterministic all-optical switching of synthetic ferrimagnets using single femtosecond laser pulses, *Phys. Rev. B* **96**, 220411 (2017).
8. J. Gorchon, C.-H. Lambert, Y. Yang, A. Pattabi, R. B. Wilson, S. Salahuddin, and J. Bokor, Single shot ultrafast all optical magnetization switching of ferromagnetic Co/Pt multilayers, *Appl. Phys. Lett.* **111**, 042401 (2017).
9. M. Vomir, M. Albrecht, and J.-Y. Bigot, Single shot all optical switching of intrinsic micron size magnetic domains of a Pt/Co/Pt ferromagnetic stack, *Appl. Phys. Lett.* **111**, 242404 (2017).
10. M. Finazzi, M. Savoini, A. R. Khorsand, A. Tsukamoto, A. Itoh, L. Duo, A. Kirilyuk, Th. Rasing, and M. Ezawa, Laser-induced magnetic nanostructures with tunable topological properties, *Phys. Rev. Lett.* **110**, 177205 (2013).
11. A. Kirilyuk, A. V. Kimel, and Th. Rasing, Ultrafast optical manipulation of magnetic order, *Rev. Mod. Phys.* **82**, 2731 (2010). Erratum *Rev. Mod. Phys.* **88**, 039904 (2016).
12. G. P. Zhang, W. Hübner, E. Beaupaire, and J.-Y. Bigot, Laser-induced ultrafast demagnetization: Femtomagnetism, A new frontier? *Topics Appl. Phys.* **83**, 245 (2002).
13. G. P. Zhang, T. Latta, Z. Babyak, Y. H. Bai, and T. F. George, All-optical spin switching: A new frontier in femtomagnetism – A short review and a simple theory, *Mod. Phys. Lett. B* **30**, 1630005 (2016).
14. M. S. El Hadri, M. Hehn, G. Malinowski, and S. Mangin, Materials and devices for all-optical helicity-dependent switching, *J. Phys. D: Appl. Phys.* **50**, 133002 (2017).
15. X. Lu, X. Zou, D. Hinzke, T. Liu, Y. Wang, T. Cheng, J. Wu., T. A. Ostler, J. Cai, U. Nowak, R. W. Chantrell, Y. Zhai, and Y. Xu, Roles of heating and helicity in ultrafast all-optical magnetization switching in TbFeCo, *Appl. Phys. Lett.* **113**, 032405 (2018).
16. T.-M. Liu *et al.*, Nanoscale confinement of all-optical magnetic switching in TbFeCo - Competition with nanoscale heterogeneity, *NanoLett.* **15**, 6862 (2015).
17. A. V. Kimel, A. Kirilyuk, A. Tsvetkov, R. V. Pisarev, and Th. Rasing, Laser-induced ultrafast spin reorientation in the antiferromagnet TmFeO<sub>3</sub>, *Nature* **429**, 850 (2004).
18. A. V. Kimel, A. Kirilyuk, P. A. Usachev, R. V. Pisarev, A. M. Balbashov, and Th. Rasing, Ultrafast non-thermal control of magnetization by instantaneous photomagnetic pulses, *Nature* **435**, 655 (2005).
19. A. V. Kimel, B. A. Ivanov, R. V. Pisarev, P. A. Usachev, A. Kirilyuk, and Th. Rasing, Inertia-driven spin switching in antiferromagnets, *Nat. Phys.* **5**, 727 (2009).
20. Z. Jin, H. Ma, L. Wang, G. Ma, F. Guo, and J. Chen, Ultrafast all-optical magnetic switching in NaTb(WO<sub>4</sub>)<sub>2</sub>, *Appl. Phys. Lett.* **96**, 201108 (2010).
21. J. Hohlfeld, C. D. Stanciu, and A. Rebel, Athermal all-optical femtosecond magnetization reversal in GdFeCo, *Appl. Phys. Lett.* **94**, 152504 (2009).
22. K. Vahaplar, A. M. Kalashnikova, A. V. Kimel, D. Hinzke, U. Nowak, R. Chantrell, A. Tsukamoto, A. Itoh, A. Kirilyuk, and Th. Rasing, Ultrafast path for optical magnetization reversal via a strongly nonequilibrium state, *Phys. Rev. Lett.* **103**, 117201 (2009).
23. D. Steil, S. Alebrand, A. Hassdenteufel, M. Cinchetti, and M. Aeschlimann, All-optical magnetization recording by tailoring optical excitation parameters, *Phys. Rev. B* **84**, 224408 (2011).
24. T. Ohkochi, H. Fujiwara, M. Kotsugi, A. Tsukamoto, K. Arai, S. Isogami, A.

28 *Zhang, Murakami, Si, Bai, and George*

- Sekiyama, J. Yamaguchi, K. Fukushima, R. Adam, C. M. Schneider, T. Nakamura, K. Kodama, M. Tsunoda, T. Kinoshita, and S. Suga, Microscopic and spectroscopic studies of light-induced magnetization switching GdFeCo facilitated by photoemission electron microscopy, *Jpn. J. Appl. Phys.* **51**, 073001 (2012).
25. K. Vahaplar, A. M. Kalashnikova, A. V. Kimel, S. Gerlach, D. Hinzke, U. Nowak, R. Chantrell, A. Tsukamoto, A. Itoh, A. Kirilyuk, and Th. Rasing, All-optical magnetization reversal by circularly polarized laser pulses: Experiment and multiscale modeling, *Phys. Rev. B* **85**, 104402 (2012).
26. A. R. Khorsand, M. Savoini, A. Kirilyuk, A. V. Kimel, A. Tsukamoto, A. Itoh, and Th. Rasing, Role of magnetic circular dichroism in all-optical magnetic recording, *Phys. Rev. Lett.* **108**, 127205 (2012).
27. S. Alebrand, A. Hassdenteufel, D. Steil, M. Cinchetti, and M. Aeschlimann, Interplay of heating and helicity in all-optical magnetization switching, *Phys. Rev. B* **85**, 092401 (2012).
28. S. Alebrand, M. Gottwald, M. Hehn, D. Steil, M. Cinchetti, D. Lacour, E. E. Fullerton, M. Aeschlimann, and S. Mangin, Light-induced magnetization reversal of high-anisotropy TbCo alloy films, *Appl. Phys. Lett.* **101**, 162408 (2012).
29. A. Hassdenteufel, B. Hebler, C. Schubert, A. Liebig, M. Teich, M. Helm, M. Aeschlimann, M. Albrecht, and R. Bratschitsch, Thermally assisted all-optical helicity dependent magnetic switching in amorphous  $\text{Fe}_{100-x}\text{Tb}_x$  alloy films, *Adv. Mater.* **25**, 3122 (2013).
30. S. Mangin, M. Gottwald, C-H. Lambert, D. Steil, V. Uhler, L. Pang, M. Hehn, S. Alebrand, M. Cinchetti, G. Malinowski, Y. Fainman, M. Aeschlimann, and E. E. Fullerton, Engineered materials for all-optical helicity-dependent magnetic switching, *Nat. Mater.* **13**, 286 (2014).
31. C. Schubert, A. Hassdenteufel, P. Matthes, J. Schmidt, M. Helm, R. Bratschitsch, and M. Albrecht, All-optical helicity dependent magnetic switching in an artificial zero moment magnet, *Appl. Phys. Lett.* **104**, 082406 (2014).
32. A. Hassdenteufel, J. Schmidt, C. Schubert, B. Hebler, M. Helm, M. Albrecht, and R. Bratschitsch, Low-remanence criterion for helicity-dependent all-optical magnetic switching in ferrimagnets, *Phys. Rev. B* **91**, 104431 (2015).
33. A. Hassdenteufel, C. Schubert, B. Hebler, H. Schultheiss, J. Fassbender, M. Albrecht, and R. Bratschitsch, All-optical helicity dependent magnetic switching in Tb-Fe thin films with a MHz laser oscillator, *Opt. Express* **22**, 10017 (2014).
34. L. Gierster, A. A. Ünal, L. Pape, F. Radu, and F. Kronast, Laser induced magnetization switching in a TbFeCo ferrimagnetic thin film: Discerning the impact of dipolar fields, laser heating and laser helicity by XPEEM, *Ultramicroscopy* **159**, 508 (2015).
35. M. S. El Hadri, M. Hehn, P. Pirro, C.-H. Lambert, G. Malinowski, E. E. Fullerton, and S. Mangin, Domain size criterion for the observation of all-optical helicity-dependent switching in magnetic thin films, *Phys. Rev. B* **94**, 064419 (2016).
36. B. Hebler, A. Hassdenteufel, P. Reinhardt, H. Karl, and M. Albrecht, Ferrimagnetic Tb-Fe alloy thin films: composition and thickness dependence of magnetic properties and all-optical switching, *Frontiers in Materials* **3**, 8 (2016).
37. C.-H. Lambert, S. Mangin, B. S. D. Ch. S. Varaprasad, Y. K. Takahashi, M. Hehn, M. Cinchetti, G. Malinowski, K. Hono, Y. Fainman, M. Aeschlimann, and E. E. Fullerton, All-optical control of ferromagnetic thin films and nanostructures, *Science* **345**, 1337 (2014).
38. R. John, M. Berritta, D. Hinzke, C. Müller, T. Santos, H. Ulrichs, P. Nieves, J. Walowski, R. Mondal, O. Chubykalo-Fesenko, J. McCord, P. M. Oppeneer, U. Nowak, and M. Müntenberg, Magnetisation switching of FePt nanoparticle recording medium

- by femtosecond laser pulses, *Sci. Rep.* **7**, 4114 (2017).
39. S. Iihama, Y. Xu, M. Deb, G. Malinowski, M. Hehn, J. Gorchon, E. E. Fullerton, and S. Mangin, Single-shot multi-level all-optical magnetization switching mediated by spin-polarized hot electron transport, arXiv 1805.02432.
  40. L. Le Guyader, M. Savoini, S. El Moussaoui, M. Buzzi, A. Tsukamoto, A. Itoh, A. Kirilyuk, T. Rasing, A.V. Kimel, and F. Nolting, Nanoscale sub-100 picosecond all-optical magnetization switching in GdFeCo microstructures, *Nat. Comm.* **6**, 5839 (2015).
  41. Y. H. Ren, W. Lai, Z. Cevher, Y. Gong, and G. P. Zhang, Experimental demonstration of 55-fs spin canting in photoexcited iron nanoarrays, *Appl. Phys. Lett.* **110**, 082404 (2017).
  42. G. P. Zhang, Y. H. Bai and T. F. George, A new and simple model for magneto-optics uncovers an unexpected spin switching, *EPL* **112**, 27001 (2015).
  43. G. P. Zhang, Y. H. Bai, and T. F. George, Switching ferromagnetic spins by an ultrafast laser pulse: Emergence of giant optical spin-orbit torque, *EPL* **115**, 57003 (2016).
  44. G. P. Zhang, Y. H. Bai and T. F. George, Is perpendicular magnetic anisotropy essential to all-optical ultrafast spin reversal in ferromagnets? *J. Phys.: Condensed Matter* **29**, 425801 (2017).
  45. C. E. Patrick, S. Kumar, K. Götze, M. J. Pearce, J. Singleton, G. Rowlands, G. Balakrishnan, M. R. Lees, P. A. Goddard, and J. B. Staunton, Field-induced canting of magnetic moments in GdCo5 at finite temperature: first-principles calculations and high-field measurements, *J. Phys.: Condens. Matter* **30**, 32LT01 (2018).
  46. M. S. El Hadri, P. Pirro, C.-H. Lambert, N. Berggaard, S. Petit-Watelot, M. Hehn, G. Malinowski, F. Montaigne, Y. Quessab, R. Medapalli, E. E. Fullerton, and S. Mangin, Electrical characterization of all-optical helicity-dependent switching in ferromagnetic Hall crosses, *Appl. Phys. Lett.* **108**, 092405 (2016).
  47. M. Albrecht, private communication.
  48. S. J. Yuan, L. Sun, H. Sang, J. Du, and S. M. Zhou, Interfacial effects on magnetic relaxation in Co/Pt multilayers, *Phys. Rev. B* **68**, 134443 (2003).
  49. G. P. Zhang, Y. H. Bai, and T. F. George, arXiv:1609.05855 (2016).
  50. V. N. Gridnev, Ferromagneticlike states and all-optical magnetization switching in ferrimagnets, *Phys. Rev. B* **98**, 014427 (2018).
  51. B. Szpunar and B. Kozarzewski, The application of CPA to calculations of the mean magnetic moment in the  $\text{Gd}_{1-x}\text{Ni}_x$ ,  $\text{Gd}_{1-x}\text{Fe}_x$ ,  $\text{Gd}_{1-x}\text{Co}_x$  and  $\text{Y}_{1-x}\text{Co}_x$  intermetallic compounds, *Phys. Stat. Sol. (b)* **82**, 205 (1977).
  52. Ph. Kurz, G. Bihlmayer, and S. Blügel, Magnetism and electronic structure of hcp Gd and the Gd(0001) surface, *J. Phys.: Condens. Matter* **14**, 6353 (2002).
  53. J. H. Mentink, J. Hellsvik, D. V. Afanasiev, B. A. Ivanov, A. Kirilyuk, A. V. Kimel, O. Eriksson, M. I. Katsnelson, and Th. Rasing, Ultrafast Spin Dynamics in Multisublattice Magnets, *Phys. Rev. Lett.* **108**, 057202 (2012).
  54. G. P. Zhang, Z. Babyak, Y. Xue, Y. B. Bai and T. F. George, First-principles and model simulation of all-optical spin reversal, *Phys. Rev. B* **96**, 134407 (2017).
  55. A. I. Figueroa, J. Bartolomé, L. M. Garca, F. Bartolom, O. Bunau, J. Stankiewicz, L. Ruiz, J. M. Gonzalez-Calbet, F. Petroff, C. Deranlot, S. Pascarelli, P. Bencok, N. B. Brookes, F. Wilhelm, A. Smekhova, and A. Rogalev, Structural and magnetic properties of granular Co-Pt multilayers with perpendicular magnetic anisotropy, *Phys. Rev. B* **90**, 174421 (2014).
  56. G. P. Zhang, Y. H. Bai, and T. F. George, Ultrafast reduction of exchange splitting in ferromagnetic nickel, *J. Phys.: Condens. Mat.* **28**, 236004 (2016).
  57. P. S. Pershan, J. P. van der Zie, and L. D. Malmstrom, Theoretical discussion of the

30 *Zhang, Murakami, Si, Bai, and George*

- inverse Faraday effect, Raman scattering, and related phenomena, *Phys. Rev.* **143**, 143 (1966).
58. Y. R. Shen, *The Principles of Nonlinear Optics*, (John Wiley & Sons, Inc., Hoboken, New Jersey, 1984).
59. H. Jang, B. Y. Kang, B. K. Cho, M. Hashimoto, D. Lu, C. A. Burns, C.-C. Kao, and J.-S. Lee, Observation of orbital order in the half-filled  $4f$  Gd compound, *Phys. Rev. Lett.* **117**, 216404 (2016).
60. Y. Yang, B. Wilson, J. Gorchon, C.-H. Lambert, S. Salahuddin, and J. Bokor, Ultrafast magnetization reversal by picosecond electrical pulses. *Sci. Adv.* **3**, e1603117 (2017).
61. S.-H. C. Baek, V. P. Amin, Y.-W. Oh, G. Go, S.-J. Lee, G.-H. Lee, K.-J. Kim, M. D. Stiles, B.-G. Park, and K.-J. Lee, Spin currents and spin-orbit torques in ferromagnetic trilayers, *Nat. Mat.* **17**, 509 (2018).
62. S. Brahim, H. Bouzar, and S. Lounis, Giant perpendicular magnetic anisotropy energies in CoPt thin films: impact of reduced dimensionality and imperfections, *J. Phys.: Condens. Matter* **28**, 496002 (2016).
63. T. H. Pham, J. Vogel, J. Sampaio, M. Vanatka, J.-C. Rojas-Sanchez, M. Bonfim, D. S. Chaves, F. Choueikani, P. Ohresser, E. Otero, A. Thiaville, and S. Pizzini, Very large domain wall velocities in Pt/Co/GdO<sub>x</sub> and Pt/Co/Gd trilayers with Dzyaloshinskii-Moriya interaction, *EPL* **113**, 6700 (2016).
64. Z. Y. Liu, Y. K. Lei and G. F. Wang, First-principles computation of surface segregation in L1<sub>0</sub> CoPt magnetic nanoparticles, *J. Phys.: Condens. Matter* **28**, 266002 (2016).
65. Z. Y. Liu and G. F. Wang, Surface magnetism of L1<sub>0</sub> CoPt alloy: First principles predictions, *J. Phys.: Condens. Matter* **29**, 355801 (2017).
66. B. Zimmermann, W. Legrand, N. Reyren, V. Cros, S. Blügel, and Albert Fert, Dzyaloshinskii-Moriya interaction at disordered interfaces from ab initio theory: robustness against intermixing and tunability through dusting, arXiv: 1808.04680v1 [cond-mat.mtrl-sci] 14 Aug (2018).
67. J.-Y. Chen, L. He, J.-P. Wang, and M. Li, All-optical switching of magnetic tunnel junctions with single subpicosecond laser pulses, *Phys. Rev. Appl.* **7**, 021001 (2017).
68. C. S. Davies, J. Janusonis, A. V. Kimel, A. Kirilyuk, A. Tsukamoto, Th. Rasing, and R. I. Tobey, Towards massively parallelized all-optical magnetic recording, *J. Appl. Phys.* **123**, 213904 (2018).